Bulgarian Chemical Communications, Volume 49, Special Edition K2, (pp. 74 – 79) 2017

Helicopter transient electromagnetic combined waveform transmitting technology for metal exploration

B. Guo*, Y. M. Zhang, J. L. Zhang, X. H. Wang, J. Z. Ding, J. X. Gao

Faculty of Information Technology, Beijing University of Technology, Beijing, China

Received August 15, 2017, Revised November 15, 2017

Aiming at the technical requirements to a Helicopter Transient ElectroMagnetic (HTEM) transmitter for metal ore exploration, a novel multi-pulse transmitter circuit based on LC resonance principle is proposed. Based on the full control characteristics of the IGBT device and the energy four-quadrant operation technology of the bridge circuit, a combined multi-pulse transmission circuit was realized, and precise driving timing was generated by the DSP module. The power control circuit transmits a multi-pulse waveform consisting of half-sine and trapezoidal wave to realize reuse of the same set of circuits. The principle and the circuit design method of multi-pulse emission were discussed in detail. The dynamic process and the circuit parameters of energy conversion in the half-sine and the trapezoidal wave were analysed. A bipolar multi-pulse transmitter prototype circuit with main pulse of 500A and trapezoidal wave of 50A was developed and verified by test experiments. The test results showed that the emission control method proposed in this paper achieves high-pulse current emission and small-pulse emission along the steep edge, the small-pulse edge is linearly turned off and the pulse duration is controllable. The validity of the proposed circuit topology was verified and the capability of HTEM transmitting system was improved.

Key words: Helicopter transient electromagnetic, Broadband, Combination waveform, LC resonance.

INTRODUCTION

Airborne electromagnetism is an effective method for prospecting in areas with complex topography such as deserts, swamps and forests because of its fast speed, efficiency and no need for surface personnel in prospection [1,2]. Because of its low cost, high resolution and good trafficability, the HTEM system has gradually become an important technical means in the field of airborne electromagnetic exploration [3-6]. The principle is that a primary magnetic field signal is transmitted through an aerial transmitting coil, a second magnetic field generated by induced eddy currents in an underground ore body is detected by a receiving coil, and underground electrical structure is estimated according to a second magnetic field signal [7] (Figure 1).

With the development of helicopter transient electromagnetic systems, it becomes more and more important to acquire detailed shallow area information while improving the system's depth sounding [2-8]. Simultaneous acquisition of deep and shallow area information in a flight requires that transmitters have wide-band excitation signal transmission capabilities as not only strong low-frequency signals are needed for deep information, but also abundant high-frequency information is needed for fine delineation of shallow geological structure [9,10]. SkyTEM achieves low-frequency large magnetic moments (30 Hz, 1 million Am^2) and high-frequency small magnetic moments (270 Hz, 0.4 million Am^2) by using different transmitting coils [11]. The two transmit modes require cooperation of transmitting coils with a specific number of turns and need two flights along the same survey line to obtain deep and shallow area information, so the field construction efficiency is low. Canadian Geotech's VTEM system makes the transmit waveform approximate square waves to provide large magnetic moments and rich high-frequency information by increasing current peaks and off-time of transmit waveform [12]. Since the transmitting coil has high perceptual characteristics, quick turn-off under high emission current will cause a very large turn-off voltage stress. Improvement in turn-off time and enhancement of transmitted magnetic moment are a paradox. It is difficult to greatly increase emission current while keeping rapid turn-off at the same time, so the transmitted magnetic moment is limited. The company's VTEM-Max system achieves a peak magnetic moment of 1.3 million Am^2 by increasing the area of transmitting coil. However, the increased area of transmitting coil leads to increased difficulty in flight control. The system can only fly in flat area with flat terrain, so its practical application is limited. The CHTEM-I system developed by Chen *et al.* [13] under the support of "863" program adopts trapezoidal wave approximate to square wave with a transmitted magnetic moment of 0.25 million Am^2. By

* To whom all correspondence should be sent:
E-mail: guobing2014 @emails.bjut.edu.cn

increasing the current turn-off speed, the system effectively increases high frequency components of the system transmit signals, but the transmitted magnetic moment is low, so it is difficult to achieve large depth in exploration. Yu *et al*. [14] achieved transmitted magnetic moment of 0.5 million Am^2 by using half-sine transmit waveforms, but still failed to solve the problem of low resolution of shallow area due to the use of half-sine waveform.

Considering the high inductive characteristics of transmitting coil and skin effect of signal propagating in the strata, the half-sine wave with strong electromagnetic field diffusion ability and easy realization of large current and rectangular wave or trapezoidal wave containing abundant frequency information are combined to transmit half-sine wave with a large magnetic moment and one or more trapezoidal waves with small magnetic moments in one transmit cycle [10]. Half-sine waves with large magnetic moment are transmitted to achieve deep exploration. The fast turn-off of small magnetic moment trapezoidal wave enables high-resolution shallow geological information. The transmitted waveform realizes deep sounding and high resolution at shallow area probing.

In recent years, based on the exploration and application of mineral resources and the needs of national energy strategy, the technology and methods of transient electromagnetic transmitted waveform control are developing rapidly. Fu *et al*. [15] realized a shaping circuit to speed up current shut-off. Li *et al*. [16] proposed a flat-topped half-sine waveform transmitting circuit for a fixed-wing transient electromagnetic system. Liu *et al*. [17] proposed an active clamp to achieve linear control of waveform edges. Yu Shengbao *et al*. [14] proposed a series resonant half-sine generation circuit based on a semi-controlled device. However, there is still no effective solution to multi-pulse combined emission. Although high current and high power pulse power supply have been widely used in other fields, for example, there are related studies and applications in the fields of laser power sources [18], photon sources [19] and particle accelerators [20], these impulse sources are generally bulky and heavy with low repetition frequency and only single pulse waveform can be transmitted, which are very difficult to be directly applied to an HTEM system.

In order to improve the exploration capability of the HTEM electromagnetic system and realize wideband emission current waveform, targeting at transmission of multi-pulse combination waveform, a multi-pulse transmitting circuit and control method suitable for the HTEM transmitter system was proposed in this paper. Based on full control characteristics of IGBT device and energy four-quadrant operation technology of bridge circuit, multi-pulse combination waveform transmitting circuit was developed. The precise drive timing was generated by DSP. The multi-pulse combination waveform composed of half-sine and trapezoidal wave enabled reuse of the same set of circuit, thus offering advantages of simple structure and high reliability.

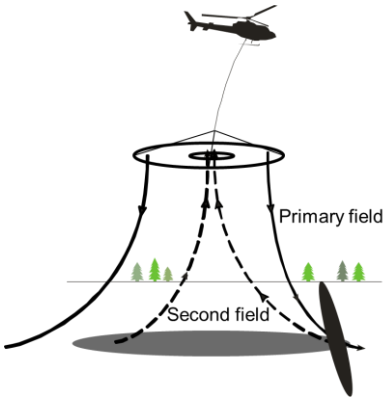

Fig. 1. HTEM operation principle.

COMBINED WAVE TRANSMITTER ARCHITECTURE

The operating principle of multi-pulse HTEM system transmitter is shown in Figure 2. The system mainly includes four parts of high-power main circuit, control unit, power management and operation interface. The high-power main circuit consists of power supply, charging circuit, resonant circuit, signal detection and drive circuit. The control unit is mainly composed of DSP control module, synchronization circuit and remote control logic. The operation interface provides user control information input, transmitter status output, synchronization signal access and transmitter remote control connection.

The functions of each part of the system are as follows: DSP control unit and the master control system have real-time data exchange to generate synchronized timing logic control signals; signal detection unit provides voltage detection and current waveform recording, temperature detection and small trapezoidal wave turn-off detection for real-time monitoring of transmitter status; driver circuit converts PWM control signal generated by DSP to IGBT gate drive signal with a certain driving ability, and fully controls opening and shutoff of IGBT; IGBT transmitting bridge is for power conversion that controls capacitor bank charging and LC resonant circuit sub-combination. The power management converts high voltage

power into voltages required for functional circuits, and safely isolates strong and weak power.

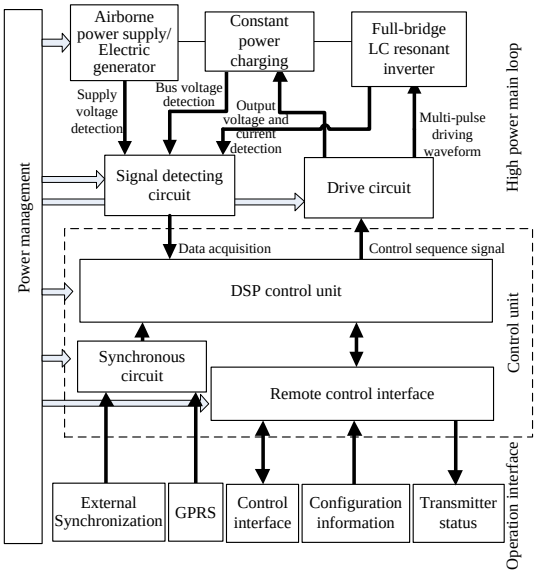

Fig. 2. Diagram of time domain multi-pulse airborne electromagnetic transmitter.

COMBINED MULTI-PULSE TRANSMITTER PRINCIPLE

It is because the shorter the turn-off delay time, the richer is the high-frequency information contained in the corresponding frequency spectrum, and the higher is the capacity of high-frequency signal, which can effectively improve system exploration ability in shallow area. As can be known from skin effect of signal, high-frequency signal decays rapidly during the propagation in strata, while low-frequency signal can penetrate the strata and reach deeper. Hence, deep exploration requires emission of low-frequency pulse with a large magnetic moment and long current duration as much as possible. It is because of the longer duration, stronger energy is sensed in subterranean medium, and the corresponding late observation signal is stronger [21].

The multi-pulse transmission control method proposed in this paper consists of a transmitting coil, a capacitor bank and an IGBT bridge circuit. The four-quadrant operation mechanism of pulse energy was used to realize multi-pulse transmission, residual energy recovery of the transmitting coil and voltage clamping on the edge of the trapezoidal wave.

The proposed multi-pulse transmitting circuit structure is shown in Figure 3, which consists of three parts: DC/DC capacitor charging circuit, storage capacitor bank C_{bank} and LC resonant bridge inverter circuit. Multi-pulse transmission waveform is shown in Figure 4, which includes half-sine main pulse and sub-waveform small trapezoidal wave. A cycle is divided into two parts of positive half cycle and negative half cycle. A cycle consists of 10 control intervals (Figure 5). Positive and negative polarity pulse have similar control mode. The following is a detailed description of the transmission process of positive-polarity wave under steady state conditions.

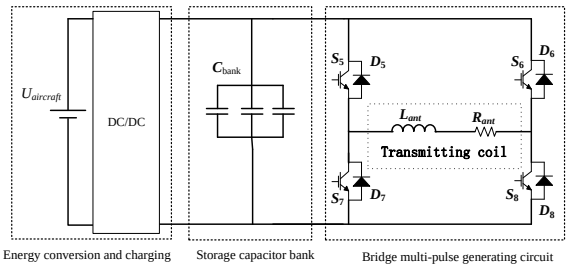

Fig. 3. Transmitter circuit topology.

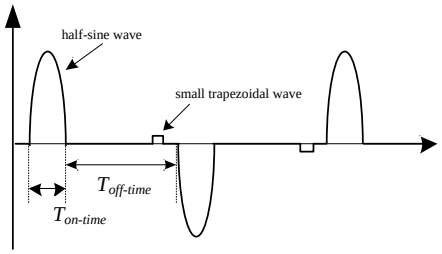

Fig. 4. Multi-pulse transmitting waveform.

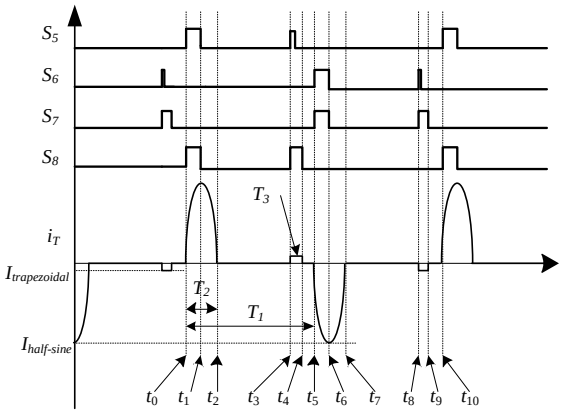

Fig. 5. Multi-pulse current generation waveform.

Before time t_0, C_{bank} is charged to voltage U_C and the charging circuit is disconnected. S_5 and S_8 are turned on at time t_0, as shown in Figure 6(a). C_{bank} and transmitting coil then form a loop, transmitting half-sine rising current waveform as shown in time period t_0 to t_1 in Figure 5. At time t_1, S_5, S_8 are closed, then transmitting coil L_{ant} constitutes a resonant circuit through D_6, D_7 and C_{bank}, and the equivalent circuit is shown in Figure 6(b) below. Half-sine drop-out current is transmitted in time period t_1 to t_2 (Figure 5). Half-sine main waveform

output is completed at time t_2. At time t_2, S_5-S_8, D_5-D_8 are turned off, charging circuit is started, so that U_{charge} charges C_{bank}, and the equivalent circuit is shown in Fig. 6(c). At time t_3, S_5, S_8 are turned on, the rising edge of the small trapezoidal wave is transmitted by the resonance of the transmitting coil and the storage inductor as shown in Figure 6(d). When the output current reaches I_2, S_5 is turned off, and a freewheeling circuit is formed through D_7, S_8, resulting in a flat top part of the small trapezoidal wave, as shown in Figure 6(e).

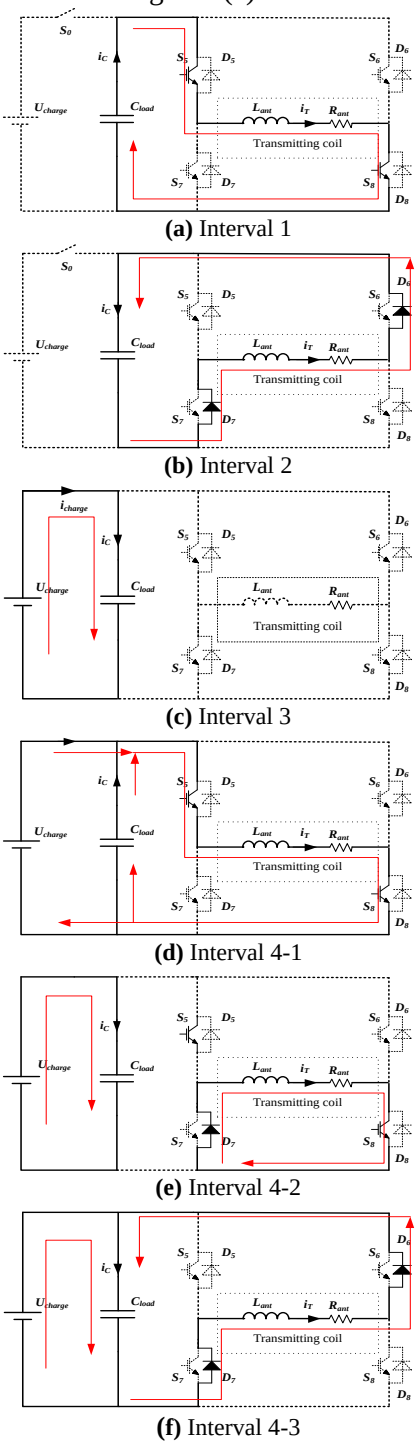

(a) Interval 1

(b) Interval 2

(c) Interval 3

(d) Interval 4-1

(e) Interval 4-2

(f) Interval 4-3

Fig. 6. Multi-pulse generation process equivalent circuit.

At time t_4, S_8 is turned off, L_{ant} and C_{bank} form a resonant circuit, resulting in falling edge of small trapezoidal wave and completing transmission of small positive trapezoidal wave, as shown in Figure 6(f).

During [t_4, t_5], U_{charge} continues to charge C_{bank}. At time t_5, voltage on both ends of C_{bank} reaches the present value U_C, and the charging circuit is turned off. Thus, positive polarity waveform transmission of the first half cycle is completed and preparation for the negative polarity half cycle is done.

EXPERIMENTAL

Experiments

According to the theoretical analysis of a multi-pulse transmission process, the experimental parameters were been deduced without considering the coupling between the transmitting coil and the earth target. Equations (1)~(3) refer to multi-pulse base frequency, duty cycle and sine wave frequency, respectively, where, T_1 is the duration of a single half-sine waveform and T_2 is the duration of a half-cycle.

$$f_{base} = 1/(2T_1) \tag{1}$$

$$D = T_2/T_1 \tag{2}$$

$$f_{\sin} = 2f_{base}/D \tag{3}$$

When S_5 and S_8 are closed, the resonant circuit equivalent circuit is shown in Figure 7. It can be drawn from the law of Huff voltage that:

$$L_{ant}C_{bank}\frac{d^2 i_T(t)}{dt^2} + R_{ant}C_{bank}\frac{di_T(t)}{dt} + i_T(t) = 0 \tag{4}$$

$$R_{ant} < 2\sqrt{L_{ant}/C_{bank}} \tag{5}$$

$$\begin{cases} L_{ant}\dfrac{di_T(t)}{dt}\Big|_{t=0} = -U_C \\ i_T(0) = 0 \end{cases} \tag{6}$$

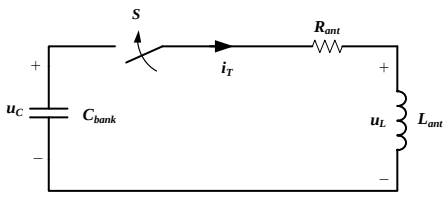

Fig. 7. Equivalent circuit at beginning resonance.

The transmitting coil is generally made of conductor with high conductivity and can easily satisfy the condition (5). According to the initial condition (6), the expression of half-sine transmitting current can be obtained:

$$i_T(t) = \frac{1}{\omega L_{ant}} U_C e^{-\delta t} \sin \omega t \tag{7}$$

where,

$$\begin{cases} \delta = \dfrac{R_{ant}}{2L_{ant}} \\ \omega = \sqrt{\dfrac{1}{L_{ant}C_{bank}} - \left(\dfrac{R_{ant}}{2L_{ant}}\right)^2} \end{cases} \tag{8}$$

When ωt = π / 2, the electric field energy stored in the capacitor can be completely converted into magnetic field energy in the transmitting coil. The peak value of the transmitting current is:

$$I_{half\text{-}sine} = \frac{U_C}{\omega L_{ant}} e^{-\delta \frac{\pi}{2\omega}} \tag{9}$$

When the loss in the loop freewheeling process is not considered, the rising and falling edge time of the small trapezoidal wave is:

$$t = \frac{1}{\omega} \arcsin \frac{I_{trapezoidal}}{I_{half\text{-}sine}} \tag{10}$$

Edge slope of the trapezoidal wave can be obtained according to the resonant current equation (9):

$$K = \frac{R_{ant}}{2L_{ant}^2} U_C \tag{11}$$

Small trapezoidal wave duration is short, and U_C descends according to the cosine curve, U_C is approximately regarded as unchanged at the initial moment of resonance, then the edge slope of the trapezoidal wave is in linear relationship with U_C.

Raw material

The detailed input and output parameters of the prototype are shown in Table 1. Precise timing control was achieved by DSP operation. The transmission of large half-sine magnetic wave was achieved by full energy exchange, and small trapezoidal waves were transmitted by voltage clamping of storage capacitor and fast switching of IGBT, and the same transmitting circuit was reused. US Tektronics oscilloscope and the corresponding high-precision current and voltage detection probes were used to measure the actual transmitted current and voltage waveform.

Table 1. Transmitter I/O

Parameter	Value
Half-sine peak current ($I_{half\text{-}sine}$)	500 A
Small trapezoidal current ($I_{trapezoidal}$)	50 A
Transmission base frequency(f_{base})	25 Hz
Main pulse duty cycle (D)	0.4
Transmitting coil radius	10 m
Transmitting coil turns	6
Transmitting coil inductance	1.98 mH

RESULTS AND DISCUSSION

According to the above multi-pulse transmission circuit principle and control method, a set of principle prototype circuit was completed, and its experimental testing and verification were done.

Figure 8 shows the current and voltage waveforms of charging and discharging of storage capacitor. Due to the large capacity of the storage capacitor bank and the use of low ESR dedicated storage capacitors, charging and discharging of current are stable, and there is no current distortion.

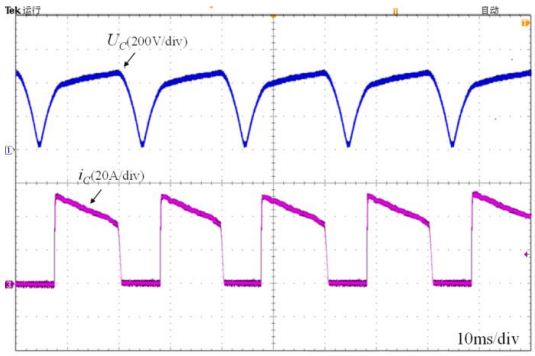

Fig. 8. C_{bank} charging current and voltage

Figure 9 shows the waveform of multi-pulse current i_T, the waveform of transmitting voltage U_T and the voltage of the storage capacitor U_C. It can be seen from the figure that during the non-transmission period $T_{off\text{-}time}$, the storage capacitor voltage is charged by the charging circuit to the preset voltage value, so that repetitive transmission at base frequency 25Hz can be well realized. Also, half-sine main waveform duty cycle can reach 0.4, half-sine main waveform peak current reaches 500A. After the transmission current reaches the peak, by controlling the IGBT switch combination, the remaining energy in the inductance of the transmitting coil is guided back to the storage capacitor.

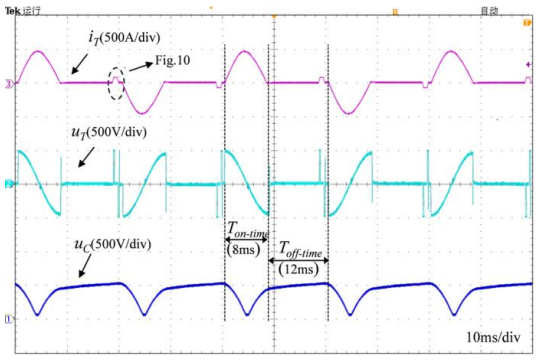

Fig. 9. Multi-pulse current and voltage.

Figure 10 shows an enlarged view of the small trapezoidal wave. Based on the experimental test

waveforms, it can be seen that the rising and trailing edge time of the small trapezoidal wave is approximately 200 μS, which is approximately linearly transformed and consistent with the theoretical analysis. During the transition between resonance and freewheeling mode, smooth current transition can be ensured without current overshoot and oscillation. The flat top current reaches 50 A, which can be effectively adjusted by controlling the time of LC resonance at the rising edge.

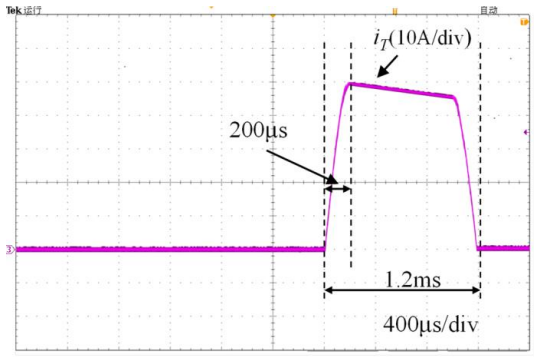

Fig. 10. Zoom-in view of the small pulse.

CONCLUSION

In order to solve the problem of wideband primary field signal transmission by a time-domain airborne electromagnetic system, a novel multi-pulse combined waveform transmission control method and circuit was proposed in this paper. Based on LC resonance and IGBT combined control technology, fast buffer and efficient recovery of transmitting coil energy was realized. More high-frequency signal components were provided under the premise of ensuring large emission current. Experimental results showed that the proposed control circuit can transmit high-quality bipolar multi-pulse waveform. Also, transmitter reliability was improved by reuse of the transmitting circuit.

Acknowledgements: *This work was supported by the Chinese Academy of Sciences Strategic pilot Technology special (class B), Grant No. XDB06030204.*

REFERENCES

1. D. Fountain, *Exploration Geophysics*, **29**, 1 (1998).
2. C.C. Yin, B. Zhang, Y.H. Liu, *Chinese J. Geophysics*, **58**, 2637 (2015).
3. W.P. Wang, Y.Y. Fang, C.P. Wu, *Chinese Journal of Engineering Geophysics*, **6**, 411 (2009).
4. S.J. Liang, L.K. Zhang, X.F. Cao, Q.K. Liu, *Geology and Exploration*, **50**, 735 (2014).
5. V. Sapia, G.A. Oldenborger, A. Viezzoli, M. Marchetti, *Journal of Applied Geophysics*, **104**, 35 (2014).
6. D. D. Massa, G. Florio, A. Viezzoli, *Journal of Applied Geophysics*, **125**, 45 (2016).
7. Y.F. Pei, C.C. Yin, Y.H. Liu, *Progress in Geophysics*, **29**, 2191 (2014).
8. J. Macnae, *Fifth Decennial International Conference on Mineral Exploration*, **387**, 1 (2007).
9. C.C. Yin, X.Y. Ren, Y.H. Liu, *Chinese J. Geophysics*, **58**, 3370 (2015).
10. T. Chen, G. Hodges, P. Miles, *Exploration Geophysics*, **46**, 49 (2015).
11. J. Reid, N. Christensen, K. Godber, *ASEG*, 2012, 1 (2012).
12. K. Tan, N. Symington, K. Lawrie, N. B. Christensen, *ASEG*, 2016, 1062 (2016).
13. B. Chen, L. F. Mao, G. D. Liu, *Chinese J. Geophys.*, **57**, 303 (2014).
14. S. Yu, Z. Han, C. Sun, Z. Zhu, J. Jiang, *Journal of Central South University (Science and Technology)* 2017, 729 (2017).
15. Z.H. Fu, J.L. Zhao, L.W. Zhou, *Chinese Journal of Scientific Instrument*, **29**, 933 (2008).
16. J.F. Li, W.J. Li, J.J. Liu, *Geophysical and Geochemical Exploration*, **38**, 1186 (2014).
17. L.H. Liu, K. Wu, Z. Geng, *Progress in Geophysics*, **31**, 0449 (2016).
18. C.K. Chana, C.C. Changa, C.L. Chena, C.S. Yanga, K.H. Hsua, Y.T. Huanga, C.K. Kuana, H.P. Hsueha, S.N. Hsua, P.J. Choua, G.Y. Hsiunga, J.R. Chenab, *Nuclear Instruments and Methods in Physics Research*, **709**, 56 (2013).
19. S.D. Jarvis, J. Mukherjee, M. Perren, S. J. Sweeney, *IET Optoelectronics*, **8**, 64 (2014).
20. K. Yoshinori, *IEEE Trans. Appl. Supercond.*, **26**, 1 (2016).
21. C.C. Yin, C.K. Qiu, Y.H. Liu, J. Cai, *Chinese J. Geophys.*, **59**, 3079 (2016).